Nanoscale Horizons

ROYAL SOCIETY OF CHEMISTRY

COMMUNICATION

View Article Online
View Journal | View Issue



Cite this: *Nanoscale Horiz.*, 2025, **10**, 1000

Received 6th December 2024,
Accepted 27th January 2025

DOI: 10.1039/d4nh00633j

rsc.li/nanoscale-horizons



# Biogenic fluorescent carbon dot-decorated mesoporous organosilica nanoparticles for enhanced bioimaging and chemotherapy†‡

Ky-Vien Le,[ab] Hanh-Vy Tran Nguyen,[ab] Phu-Quan Pham,[bc] Ngoc Hong Nguyen,[bc] Tan Le Hoang Doan,[ab] Linh Ho Thuy Nguyen,[be] Bach Thang Phan,[ab] Lan Thi My Nguyen,*[bd] Sungkyun Park,[f] Ngoc Kim Pham,*[bc] Philip Anggo Krisbiantoro,[g] Kevin C.-W. Wu*[ghi] and Ngoc Xuan Dat Mai*[ab]

**Hybrid materials possess the unique properties of their individual components, enabling their use in multiple synergistic applications. In this study, we synthesized biogenic fluorescent carbon dots (CDs) decorated with biodegradable periodic mesoporous organosilica nanoparticles (BPMO), creating BPMO@CDs. The CDs, approximately 9.8 nm in diameter, were derived from *Musa paradisiaca* cv. *Awak* juice using a rapid microwave method, exhibiting a spherical shape and green and red luminescence. The resulting BPMO@CDs are spherical, around 100 nm in size, and maintain high pore volume and surface area. The elemental chemical state in the BPMO@CDs remains consistent with that of pure BPMO. Our findings demonstrate that BPMO@CDs achieve efficient cellular uptake rates of 46.74% in MCF7 cells and 17.07% in L929 cells, with preserved fluorescence within the cells. The optical properties of the CDs are retained in the BPMO@CDs, allowing for detection upon cellular uptake. Additionally, when loaded with anticancer drugs, the BPMO@CDs significantly enhance the cytotoxicity against MCF7 breast cancer cells, highlighting their potential for synergistic bioimaging and chemotherapy applications.**

### New concepts

We report the green synthesis of fluorescent carbon dots (CDs) from banana (*Musa paradisiaca* cv. *Awak*) juice using a rapid microwave technique. These CDs are subsequently incorporated into biodegradable periodic mesoporous organosilica nanoparticles (BPMO) *via* the sol–gel method to form hybrid nanomaterials, BPMO@CDs. The hybrid materials exhibit high porosity, strong luminescence, low cytotoxicity, increased loading capacity, and enhanced toxicity toward cancer cells, demonstrating their potential for biomedical applications. For instance, we demonstrate that BPMO@CDs achieve efficient cellular uptake in MCF7 and L929 cells, with preserved fluorescence within the cells. The optical properties of the CDs are retained in the BPMO@CDs, allowing for detection upon cellular uptake. Additionally, when loaded with anticancer drugs, BPMO@CDs significantly enhance the cytotoxicity against MCF7 breast cancer cells, highlighting their potential for synergistic bioimaging and chemotherapy applications. This study provides a new concept of using environmentally friendly, biocompatible hybrid nanomaterials with potential for biomedical applications, particularly in bioimaging and drug delivery.

Bioimaging enables the real-time observation of biological processes by fusing functional information such as electric and magnetic fields, mechanical motion, metabolism, and anatomical structure. It offers a non-invasive approach to obtaining comprehensive insights into the human body's inner workings, providing detailed 3D structures without impeding natural biological activities.[1] Some materials capable of fluorescence and applied in bioimaging include PbS,[2] CdS,[2] Ag NPs,[3] Au NPs,[4] graphene,[5] and carbon dots.[6] Since its first discovery in 2004, carbon dots (CDs) have exhibited prominent advantages, such as stable luminescence, low toxicity, and simple, environmentally friendly fabrication processes,[7] making them

[a] *Center for Innovative Materials and Architectures (INOMAR), Ho Chi Minh City, Vietnam. E-mail: mnxdat@inomar.edu.vn*
[b] *Vietnam National University, Ho Chi Minh City, Vietnam*
[c] *Faculty of Materials Science and Technology, University of Science, Ho Chi Minh City, Vietnam*
[d] *Faculty of Biology and Biotechnology, University of Science, Ho Chi Minh City, Vietnam*
[e] *Faculty of Pharmacy, University of Health Sciences (UHS), Ho Chi Minh City, Vietnam*
[f] *Department of Physics, Pusan National University, Busan, South Korea*
[g] *Department of Chemical Engineering, National Taiwan University, Taipei 10617, Taiwan. E-mail: kevinwu@ntu.edu.tw*
[h] *Department of Chemical Engineering and Materials Science, Yuan Ze University, Chung-Li, Taoyuan, Taiwan*
[i] *Institute of Biomedical Engineering and Nanomedicine, National Health Research Institute, Keyan Road, Zhunan, Miaoli City 350, Taiwan*

† Congratulations to Vietnam National University Ho Chi Minh City on its 30th Anniversary (1995–2025).

‡ Electronic supplementary information (ESI) available. See DOI: https://doi.org/10.1039/d4nh00633j

promising materials. It has been extensively applied in various biomedical fields, including gene delivery,[8,9] tissue engineering,[10] biosensors,[11] antibacterials,[12,13] and particularly drug delivery,[14] cancer therapy,[15,16] and especially bioimaging.[14,17] For green synthesis approaches, countless sources of materials from plants, fruits, and bananas are widely utilized for synthesizing CDs. Bananas are commonly employed as a precursor for synthesizing CDs or carbon quantum dots (CQDs). Specific studies, such as that by De *et al.*, have utilized banana (*Musa acuminata*) juice for the synthesis of carbon dots,[18] while N, S co-doped CQDs have also been derived from banana (*Musa acuminata*) juice.[19] In addition to banana juice, the pseudo-stem of the banana plant has been used for carbon dot synthesis,[20] and CQDs have been synthesized from banana peel.[21] Furthermore, because of their small size, CDs can pass through ion channels, the glomerular filtration barrier, and the blood–brain barrier and reach cells *in vivo*.[22] On the downside, the limitations of mass, small particle size, nonspecific fluorescence, and aggregation luminescence quenching have restricted the applications of CDs in specific fields.[23] To tackle this drawback, composites of nanocarriers, such as liposomes,[24–26] micelles,[23,27] dendrimers,[28,29] metal–organic frameworks,[30,31] chitosan,[32,33] polymer,[34,35] and silica,[36–38] with CDs have shown encouraging potential as alternatives.[39]

Among the mentioned materials, mesoporous silica nanoparticles (MSNs), with their prominent characteristics such as high surface area, porous structure, and biocompatibility, by and large, have garnered attention. Nevertheless, MSNs, being inherently inorganic and difficult to degrade, are still assumed to exhibit poor degradation, tendency to accumulate, and prolonged clearance, leading to long-term toxicity in tissues and organs. Consequently, numerous articles and studies have emerged focusing on enhancing degradation capabilities through surface area tuning, surface modification, and silica framework tuning.[40] In this context, biodegradable periodic mesoporous organosilica (BPMO), a type of MSN with a tunable silica framework, has been researched to enhance its biodegradability, relying on organic functional groups attached to the silica framework to form Si–O–Si bonds, facilitating the material's biodegradation.[31] BPMO has chemically biodegradable linkages, including di- and tetra-sulfide bonds,[41] while organic R groups within the framework can also enhance drug loading and release capabilities through interactions between the drug and nanoparticles.[42] Contrariwise, studies on BPMO loaded with CDs are rare and have not been thoroughly investigated. Consequently, the composite of CDs with BPMO is used as a nanocarrier in synergistic bioimaging and chemotherapy applications, which will be the focus of this paper.

In this work, we conducted the green synthesis process of fluorescent carbon dots (CDs) from banana (*Musa paradisiaca* cv. *Awak*) juice through a microwave method that is much quicker and more convenient. For the first time, the synthesized CDs are incorporated into BPMO *via* the sol–gel method, forming BPMO@CDs. The physicochemical properties of the obtained BPMO@CDs are characterized by Fourier-transformed infrared spectroscopy (FTIR), powder X-ray diffraction (P-XRD), field emission scanning electron microscopy (FE-SEM), transmission electron microscopy (TEM), thermogravimetric analysis (TGA), X-ray photoelectron spectroscopy (XPS), and nitrogen adsorption–desorption isotherms. The fluorescence properties of the obtained nanoparticles are indicated by photoluminescence and UV-Vis spectroscopy, showing green and red fluorescence under appropriate excitation light. Furthermore, their effective internalization into MCF7 breast cancer cells and tracking ability *via* fluorescence are also demonstrated. Additionally, the biocompatibility and cytotoxicity of anticancer drug-loaded BPMO@CDs toward L929 fibroblast cells and MCF7 breast cancer cells indicated the promise of BPMO@CDs in the synergetic applications of bioimaging and chemotherapy.

## Results and discussion

A multifunctional nanoparticle was observed by combination of biodegradable organosilica with biosynthesized carbon dots (CDs), namely BPMO@CDs (Fig. 1a). These obtained particles exhibit a high porous structure and fluorescence capabilities under excitation light.

### Morphology and microstructure of BPMO@CDs

SEM images display a spherical morphology with an average size of approximately 112 nm of the BPMO@CDs particles. Their surfaces appear rough, resulting from the adherence and dispersion of CDs within the BPMO (Fig. S1, ESI‡). The clear morphology of the CDs is obtained in the TEM images with spherical-shaped and relatively uniform sizes, approximately 5 to 15 nm. Like the SEM result, the increase in size from 50 nm to 100 nm demonstrated the attachment of CDs onto the BPMO, bringing about a rougher surface (Fig. 1b–d).

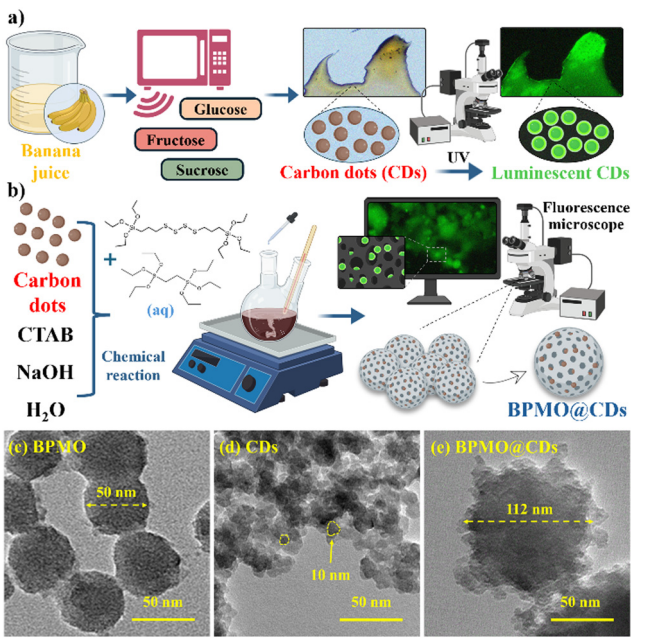


Fig. 1 A schematic of the (a) CD and (b) BPMO@CD synthesis process. TEM images of (c) BPMO, (d) CDs and (e) BPMO@CDs.

Specific vibrational signals representative of functional groups are observed in the FT-IR spectra. The vibration at 1634 $cm^{-1}$ may be attributed to C=C and C=O bonds attached to the CDs on the material's surface.[43] Furthermore, a signal indicative of C–O–C bond vibrations is found at 1413 $cm^{-1}$. Additionally, $CH_2$ group vibrations appear at 2926 $cm^{-1}$, and $CH_2$ rocking vibrations are observed at 1413 $cm^{-1}$.[44] The signals at 1271 $cm^{-1}$ and 1043 $cm^{-1}$ correspond to C–O stretching vibrations of the remaining C2/C3 carbohydrate chains.[45] A distinctive signal at 909 $cm^{-1}$ is characteristic of epoxy ring vibrations of CDs attached to BPMO.[46] Moreover, the stretching vibration of Si–O–Si bonds is also noted at this 909 $cm^{-1}$ position.[31] Similar to CDs, the presence of –OH and C–O functional groups in BPMO@CDs enhances their dispersibility in solvents.[19] The N–H and C=O functional groups observed contribute to surface states, playing a role in the luminescent properties of the material. Particularly noteworthy is that the FTIR spectra of BPMO@CDs exhibit an inheritance of signals, combining the characteristics of both source materials.

Based on the P-XRD results, the correlation peaks in the angular range of 10–40° indicate the preferential orientation

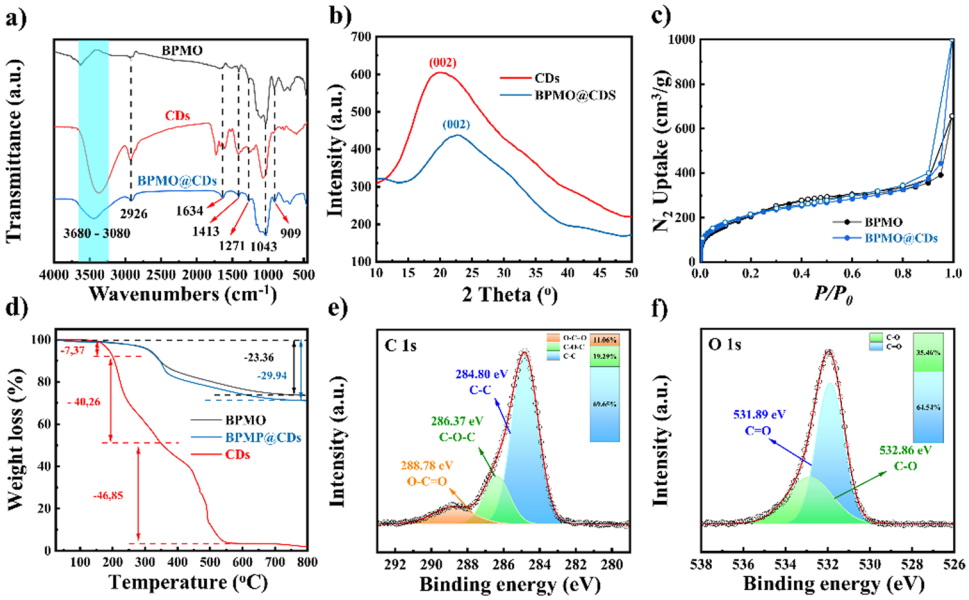


Fig. 2 Characterization of the BPMO (black), BPMO@CDs (blue), and CDs (red). (a) FTIR spectra; (b) P-XRD pattern; (c) the $N_2$ isotherms (BET) at 77 K. Solid and hollow circles correspond to adsorption and desorption results; (d) the TGA curve. Deconvoluted XPS spectra and the area ratio of BPMO@CDs for (e) C 1s and (f) O 1s.

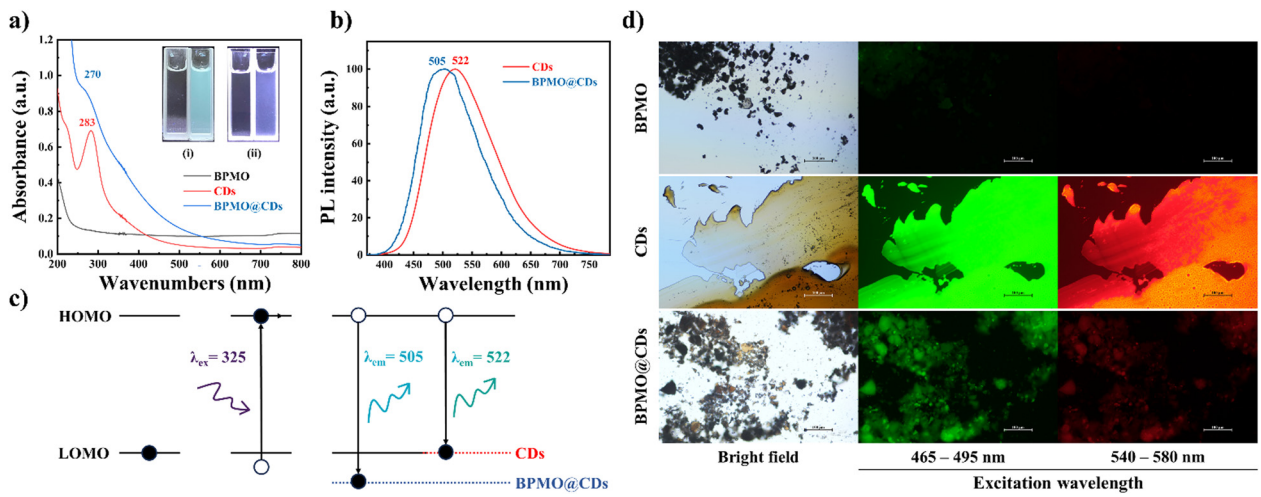


Fig. 3 (a) UV-Vis spectra of BPMO, CDs, and BPMO@CDs. Two inset images depicting water (left), CDs (i) (right), and BPMO@CDs (ii) (right) under excitation light with a wavelength of 365 nm; (b) PL spectrum of CDs and BPMO@CDs excited by light sources with wavelengths of 325 nm; (c) possible mechanism leading to the luminescent properties of CDs and BPMO@CDs; (d) the fluorescence images of BPMO, CDs, and BPMO@CDs under fluorescence microscopy with transmitted light and excitation light at 465–495 nm, and 540–580 nm.

 

along the (002) direction of CDs within the BPMO@CDs (Fig. 2b). The prominent diffraction peak at $2\theta \sim 22.90^{\circ}$ corresponds to the (002) plane, revealing an interlayer spacing of approximately 0.388 nm. This result closely aligns with the



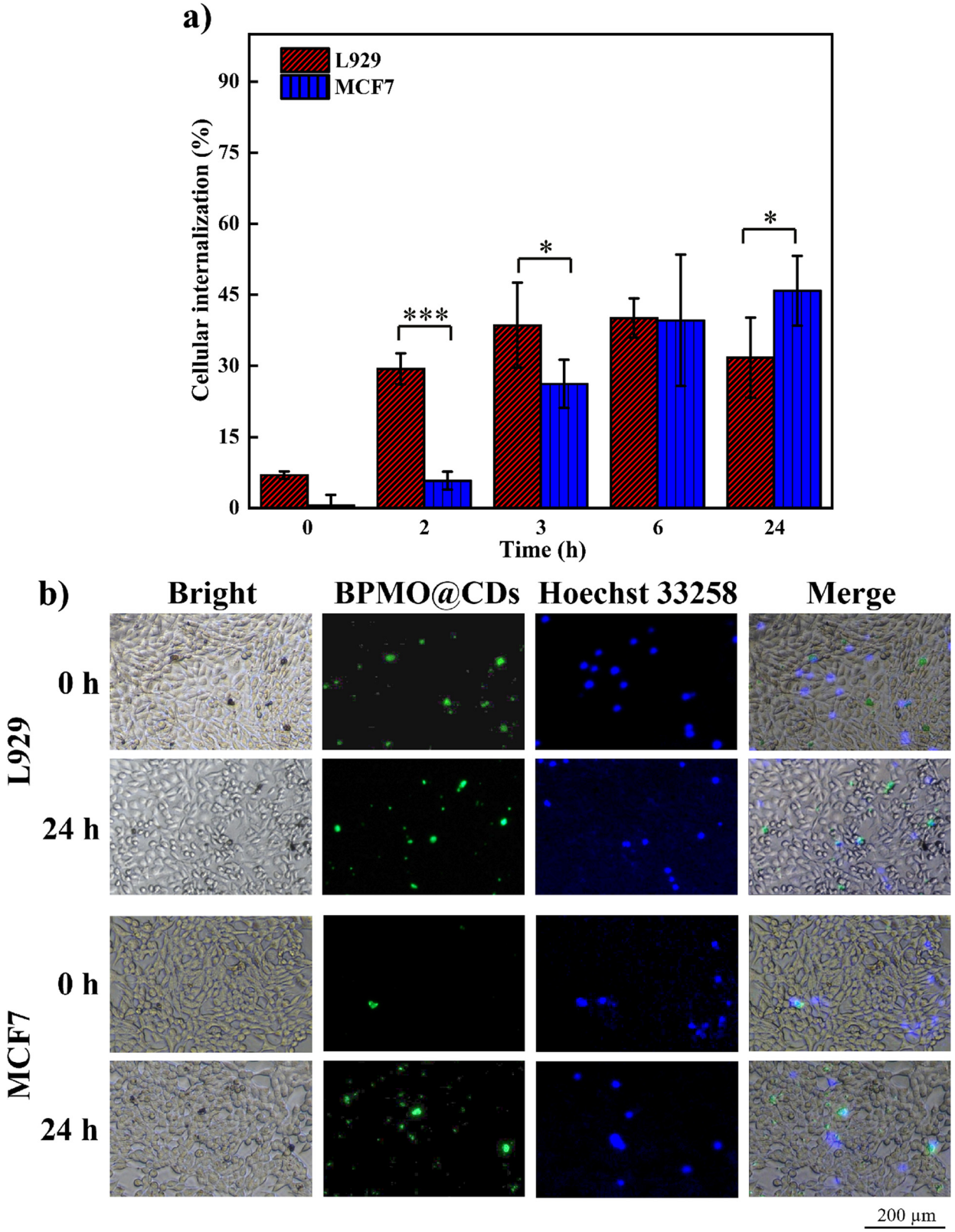


Fig. 4 (a) Percentage of cellular internalization of BPMO@CDs into L929 and MCF7 cells. The data were expressed as mean ± SD with $n = 3$ and $^{*}p < 0.05$ and $^{***}p < 0.001$; (b) fluorescence images of L929 cells and MCF7 cells incubated with BPMO@CDs.

CDs obtained using the microwave method with $2\theta$ = 21.20°. The observed slight deviation (1.7°) in the diffraction peak suggests that CDs have infiltrated into the BPMO, indicating the successful binding of CDs to the BPMO particles while preserving the structural integrity of the CDs. In addition, the nitrogen adsorption–desorption isotherms of BPMO@CDs fit a type IV isotherm, which indicates that the mesoporous structure of BPMO is still retained after attachment with CDs (Fig. 2c). The surface area slightly reduced from 793.75 $m^2 g^{-1}$ to 770.91 $m^2 g^{-1}$. The TGA curve of the BPMO@CDs shows no significant difference, mirroring the curve of BPMO. Beyond 350 °C, the TGA of the BPMO@CDs exhibits a slight decrease in weight (less than 2%) compared to the initial BPMO due to the gradual decomposition of CDs binding to the BPMO (Fig. 2d).

The XPS spectrum of BPMO@CDs also demonstrates that the chemical state of BPMO@CDs is not significantly different from BPMO, with only a minor change observed: an additional peak appears at 288.78 eV, indicating the C═O bond (Fig. 2e, f and Fig. S2, Table S1, ESI‡). Additionally, the elemental analysis results show the higher carbon content in BPMO@CDs (20.36%) compared to 18.94% of BPMO (Table S2, ESI‡).

### Optical properties of BPMO@CDs

In Fig. 3a, the CDs reveal a distinctive peak at 283 nm.[47] Conversely, BPMO lacks any discernible absorption peak, resulting in a blue shift in the absorption peak of BPMO@CDs, manifesting a peak at 270 nm. CDs (i) exhibit green fluorescence upon exposure to 365 nm excitation light. In BPMO@CDs (ii), the minute particles emit a subtle green fluorescence but overall look like they fluoresce purple. This phenomenon can be elucidated by considering the structural arrangement in BPMO@CDs, where CDs adhere and disperse into the BPMO structure. Given that the BPMO material possesses a white color, 365 nm UV light (appearing as purple) induces reflective interference, causing the purple fluorescence to mask the intrinsic green fluorescence of the CDs. The luminescent characteristics of BPMO@CDs will be more distinctly elucidated through fluorescence microscope imagery.

The photoluminescence spectrum (PL) results (Fig. 3b) reveal the maximum fluorescence peaks in the green region, specifically at 505 nm and 522 nm, corresponding to CDs and BPMO@CDs when excited with light at 325 nm. From the absorption peaks in the UV-Vis results, it can be observed that the absorption peak of CDs ($\lambda_{max}$ = 283 nm) is greater than that of BPMO@CDs ($\lambda_{max}$ = 270 nm). Based on the photon energy formula $E = hf = hc/\lambda$, this paper proposes that the bandgap of BPMO@CDs molecules is smaller than that of CD molecules. As the bandgap ($E_g$) increases, the emitted energy also increases. Under the excitation energy, due to the smaller $E_g$ of CDs compared to $E_g$ of BPMO@CDs, the emission energy of BPMO@CDs may be greater than the emission energy of CDs. Consequently, it can be explained why BPMO@CDs, translating to a shorter wavelength, exhibit a lower photoluminescence peak at $\lambda_{PL}$ = 505 nm compared to CDs at $\lambda_{PL}$ = 522 nm. Fig. 3c illustrates the possible mechanism that could lead to the luminescent properties of CDs and BPMO@CDs.

The fluorescence properties of hybrid materials are clearly observed when exposed to the excitation light. In detail, BPMO@CDs exhibit vivid and distinct green and red fluorescence that results from CDs. However, their fluorescence intensity is not as strong and vibrant as that of pure CDs (Fig. 3d).

### Internalization of BPMO@CDs

Fig. 4a illustrates the percentage of BPMO@CDs internalization into L929 fibroblast cells and MCF7 breast cancer cells at different time points (0, 2, 3, 6, and 24 hours). The results indicate a gradual increase in nanoparticle uptake over time, with the highest uptake observed after 24 hours of treatment. At the initial time points (0, 2, and 3 hours), L929 cells exhibited higher nanoparticle absorption compared to MCF7 cells. However,

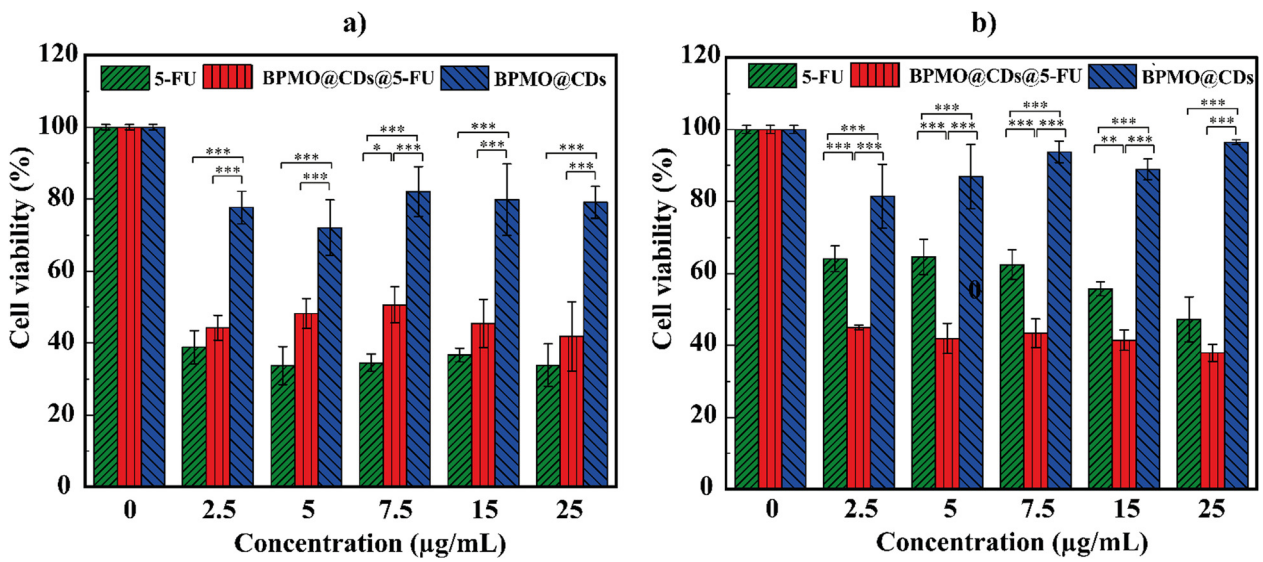


Fig. 5 The cell viability of anticancer drug 5-fluorouracil (5-FU), BPMO@CDs, and BPMO@CDs@5-FU with (a) L929 fibroblast normal cells and (b) MCF7 breast cancer cells using the MTT assay. The data were expressed as mean ± SD with $n$ = 3 and *$p < 0.05$, **$p < 0.01$ and ***$p < 0.001$.

 

at 6 hours, both cell lines demonstrated a similar uptake of approximately 40%. After 24 hours, the uptake in MCF7 cells reached 45.85%, surpassing that of L929 cells, which was only 31.75%.

Fluorescence images of L929 and MCF7 cells incubated with BPMO@CDs are displayed in Fig. 4b. The nuclei are stained blue with Hoechst, while the BPMO@CDs exhibit green fluorescence. After 24 hours, the MCF7 cells showed a more intense and widespread green fluorescence signal compared to L929 cells, indicating higher nanoparticle uptake by cancer cells. This observation aligns with the quantitative uptake data presented in Fig. 4a.

### Cytotoxicity

The toxicity of free 5-FU, BPMO@CDs, and BPMO@CDs@5-FU on the proliferation of L929 fibroblast normal cells and MCF7 breast cancer cells is investigated. The calculated loading capacity of 5-FU into BPMO@CDs was 136.6 mg $g^{-1}$. As shown in Fig. 5, the BPMO@CDs show no considerable toxicity on both cell lines, L929 and MCF7, due to cell viability $>70\%$. This demonstrated the biocompatibility of BPMO@CDs with the corresponding concentration on normal cells. On the other hand, the cytotoxicity of 5-FU on MCF7 is increased when loaded into BPMO@CDs. Cell viability gradually decreases when the concentration of BPMO@CDs@5-FU is increased, reaching over 40% of cell viability. Furthermore, these efficiencies are higher than those of free 5-FU, indicating the efficiency of BPMO@CDs in increasing the toxicity of 5-FU and then can be used as a useful delivery system.

From all the obtained results, BPMO@CDs can be used as multifunctional nanoparticles with BPMO as a nanocarrier due to high porosity and CDs with strong luminescence. Hence, BPMO@CDs are introduced for potential applications in the field of biomedical sciences, particularly in bioimaging and drug delivery.

## Conclusions

To summarize, we have successfully synthesized a biogenic fluorescent carbon dot-decorated porous organosilica nanoparticle by combining fluorescent CDs biosynthesized from *Musa paradisiaca* cv. *Awak* spherical particles with BPMO. When exposed to the excitation light, the green synthesized carbon dots exhibit strong fluorescence properties. This fluorescence capability remained when incorporated into BPMO, leading to usability in advanced bioimaging. In addition, hybrid BPMO@CDs can increase the cytotoxicity of the 5-FU anticancer drug toward MCF7 breast cancer cells as a carrier. These hybrid BPMO@CDs exhibit high porosity, strong luminescence, low cytotoxicity, increased loading capacity, and toxicity toward cancer cells, demonstrating the potential for biomedical sciences, particularly in bioimaging and drug delivery.

## Data availability

The data supporting this article have been included as part of the ESI‡ and can be found in the online version.

## Conflicts of interest

There are no conflicts to declare.

## Acknowledgements

This study was supported by the Vietnam National University, Ho Chi Minh City under grant number TX2025-50-01.

## References

1 H. S. Lahoti and S. D. Jogdand, *Cureus*, 2022, **14**, e28923.
2 X. Qiu, X. Zhu, X. Su, M. Xu, W. Yuan, Q. Liu, M. Xue, Y. Liu, W. Feng and F. Li, *Adv. Sci.*, 2019, **6**, 1801834.
3 M. T. Yaraki, Y. Pan, F. Hu, Y. Yu, B. Liu and Y. N. Tan, *Mater. Chem. Front.*, 2020, **4**, 3074–3085.
4 P. Si, N. Razmi, O. Nur, S. Solanki, C. M. Pandey, R. K. Gupta, B. D. Malhotra, M. Willander and A. de la Zerda, *Nanoscale Adv.*, 2021, **3**, 2679–2698.
5 R. Kumar, D. P. Singh, R. Muñoz, M. Amami, R. K. Singh, S. Singh and V. Kumar, *Mater. Today Chem.*, 2023, **33**, 101750.
6 M. M. Hussain, W. U. Khan, F. Ahmed, Y. Wei and H. Xiong, *Chem. Eng. J.*, 2023, **465**, 143010.
7 P. Zhu, S. Wang, Y. Zhang, Y. Li, Y. Liu, W. Li, Y. Wang, X. Yan and D. Luo, *ACS Appl. Bio Mater.*, 2022, **5**, 2031–2045.
8 M. Algarra González and E. González-Muñoz, *Biol. Proced. Online*, 2024, **26**, 6.
9 Q. Wang, L. Shi, J. Zhao and S. Shuang, *Appl. Surf. Sci.*, 2022, **599**, 153902.
10 N. Farshidfar, S. Fooladi, M. H. Nematollahi and S. Iravani, *RSC Adv.*, 2023, **13**, 14517–14529.
11 Y. Yang, C. Wang, Q. Shu, N. Xu, S. Qi, S. Zhuo, C. Zhu and J. Du, *Spectrochim. Acta, Part A*, 2022, **268**, 120681.
12 Z. X. Wang, Z. Wang and F. G. Wu, *ChemMedChem*, 2022, **17**, e202200003.
13 L.-N. Wu, Y.-J. Yang, L.-X. Huang, Y. Zhong, Y. Chen, Y.-R. Gao, L.-Q. Lin, Y. Lei and A.-L. Liu, *Carbon*, 2022, **186**, 452–464.
14 P. Jana and A. Dev, *Mater. Today Commun.*, 2022, **32**, 104068.
15 L. Yu, Y. Wang, K. Li, X. Li, M. He, C. Chen, F. Li, B. Liang, L. Li and N. Gu, *Carbon*, 2023, **212**, 118095.
16 Y. Xu, B. Wang, M. Zhang, J. Zhang, Y. Li, P. Jia, H. Zhang, L. Duan, Y. Li and Y. Li, *Adv. Mater.*, 2022, **34**, 2200905.
17 G. Gedda, S. A. Sankaranarayanan, C. L. Putta, K. K. Gudimella, A. K. Rengan and W. M. Girma, *Sci. Rep.*, 2023, **13**, 6371.
18 B. De and N. Karak, *Rsc Adv.*, 2013, **3**, 8286–8290.
19 N. Chaudhary, P. K. Gupta, S. Eremin and P. R. Solanki, *J. Environ. Chem. Eng.*, 2020, **8**, 103720.
20 S. A. A. Vandarkuzhali, V. Jeyalakshmi, G. Sivaraman, S. Singaravadivel, K. R. Krishnamurthy and B. Viswanathan, *Sens. Actuators, B*, 2017, **252**, 894–900.
21 R. Atchudan, T. N. J. I. Edison, M. Shanmugam, S. Perumal, T. Somanathan and Y. R. Lee, *Phys. E*, 2021, **126**, 114417.

22 B. Wang, H. Cai, G. I. Waterhouse, X. Qu, B. Yang and S. Lu, *Small Sci.*, 2022, **2**, 2200012.
23 J. Li, Y. Yang and P. Liu, *Mol. Pharmaceutics*, 2023, **20**, 1426–1434.
24 B. Demir, H. Moulahoum, F. Ghorbanizamani, F. B. Barlas, O. Yesiltepe, Z. P. Gumus, K. Meral, D. O. Demirkol and S. Timur, *J. Drug Delivery Sci. Technol.*, 2021, **62**, 102363.
25 S.-C. Wei, A. Nain, Y.-F. Lin, R.-S. Wu, P. Srivastava, L. Chang, Y.-F. Huang, H.-T. Chang, K.-T. Chuang and C.-C. Huang, *Carbon*, 2023, **201**, 952–961.
26 H. Faghihi, M. Mozafari, A. Bumrungpert, H. Parsaei, S. V. Taheri, P. Mardani, F. M. Dehkharghani, M. Y. Pudza and M. Alavi, *Photodiagn. Photodyn. Ther.*, 2023, **42**, 103614.
27 A. Xu, H. Liu, J. Zhang and H. Li, *Chem. Commun.*, 2023, **59**, 13871–13874.
28 Y. Guo, M. Shen and X. Shi, *Macromol. Biosci.*, 2021, **21**, 2100007.
29 P. Wolski, T. Panczyk and A. Brzyska, *J. Phys. Chem. C*, 2023, **127**, 16740–16750.
30 S. H. Nannuri, A. Pandey, S. Kulkarni, P. K. Deshmukh, S. D. George and S. Mutalik, *Mater. Today Commun.*, 2023, **35**, 106340.
31 T. T. T. Nguyen, B. Q. G. Le, M.-H. D. Dang, B. T. Phan, N. X. D. Mai and T. L. H. Doan, *Microporous Mesoporous Mater.*, 2022, **338**, 111944.
32 S. A. Mathew, P. Praveena, S. Dhanavel, R. Manikandan, S. Senthilkumar and A. Stephen, *RSC Adv.*, 2020, **10**, 24386–24396.
33 A. M. Villalba-Rodríguez, R. B. González-González, M. Martínez-Ruiz, E. A. Flores-Contreras, M. F. Cárdenas-Alcaide, H. M. Iqbal and R. Parra-Saldívar, *Mar. Drugs*, 2022, **20**, 782.
34 Q. Liu, S. Xu, C. Niu, M. Li, D. He, Z. Lu, L. Ma, N. Na, F. Huang and H. Jiang, *Biosens. Bioelectron.*, 2015, **64**, 119–125.
35 Z. Feng, K. H. Adolfsson, Y. Xu, H. Fang, M. Hakkarainen and M. Wu, *Sustainable Mater. Technol.*, 2021, **29**, e00304.
36 M. Akbarian, M. Gholinejad, S. Mohammadi-Samani and F. Farjadian, *Microporous Mesoporous Mater.*, 2022, **329**, 111512.
37 M. P. Shirani, A. A. Ensafi, B. Rezaei and Z. Amirghofran, *J. Iran. Chem. Soc.*, 2023, **20**, 2257–2268.
38 A. A. Kajani, L. Rafiee, S. H. Javanmard, N. Dana and S. Jandaghian, *RSC Adv.*, 2023, **13**, 9491–9500.
39 N. B. Fernandes, Y. Nayak, S. Garg and U. Y. Nayak, *Coord. Chem. Rev.*, 2023, **478**, 214977.
40 A. Lérida-Viso, A. Estepa-Fernández, A. García-Fernández, V. Martí-Centelles and R. Martínez-Máñez, *Adv. Drug Delivery Rev.*, 2023, 115049.
41 F. Tamanoi, S. Chinnathambi, M. Laird, A. Komatsu, A. Birault, T. Takata, T. L.-H. Doan, N. X. D. Mai, A. Raitano and K. Morrison, *Int. J. Mol. Sci.*, 2021, **22**, 2251.
42 S. Chinnathambi and F. Tamanoi, *Pharmaceutics*, 2020, **12**, 890.
43 S. Rodríguez-Varillas, T. Fontanil, Á. J. Obaya, A. Fernández-González, C. Murru and R. Badía-Laíño, *Appl. Sci.*, 2022, **12**, 773.
44 Z. Liu, M. Chen, Y. Guo, J. Zhou, Q. Shi and R. Sun, *Chem. Eng. J.*, 2020, **384**, 123260.
45 M. He, J. Zhang, H. Wang, Y. Kong, Y. Xiao and W. Xu, *Nanoscale Res. Lett.*, 2018, **13**, 1–7.
46 Y.-H. Hsu, H.-L. Hsieh, G. Viswanathan, S. H. Voon, C. S. Kue, W. S. Saw, C. H. Yeong, C. A. Azlan, T. Imae and L. V. Kiew, *J. Nanopart. Res.*, 2017, **19**, 1–19.
47 Y. Sun, T. Yue, Y. Yuan and Y. Shi, *eFood*, 2023, **4**, e65.

 